JGR Solid Earth

RESEARCH ARTICLE
10.1029/2021JB022157

Quantitative Thermal Emission Spectroscopy at High Temperatures: A Laboratory Approach for Measurement and Calibration

James O. Thompson[1,2], Daniel B. Williams[1], Rachel J. Lee[3], and Michael S. Ramsey[1]

[1]Department of Geology and Environmental Science, University of Pittsburgh, Pittsburgh, PA, USA, [2]Department of Geosciences, Baylor University, Waco, TX, USA, [3]Department of Atmospheric and Geological Sciences, SUNY Oswego, Oswego, NY, USA

Key Points:

- Calibrated, high temperature (<1,573 K) middle infrared (MIR) and thermal infrared (TIR) laboratory emission spectra are presented, with high measurement accuracy and certainty
- Forsterite and quartz were used for calibration testing over a large temperature range, indicating polymorphic changes and amorphization
- A Hawaiian basalt shows emissivity increasing by <60% during cooling, a significant difference from prior studies that assumed no changes

Correspondence to:
J. O. Thompson,
james.thompson@pitt.edu

Citation:
Thompson, J. O., Williams, D. B., Lee, R. J., & Ramsey, M. S. (2021). Quantitative thermal emission spectroscopy at high temperatures: A laboratory approach for measurement and calibration. *Journal of Geophysical Research: Solid Earth*, *126*, e2021JB022157. https://doi.org/10.1029/2021JB022157

Received 31 MAR 2021
Accepted 23 JUN 2021

Abstract Acquiring accurate high temperature laboratory-based infrared emission spectra of geologic samples is important to constrain their radiative and spectral properties. This is important in calculations of lava flow cooling, crust formation, and ultimately lava flow propagation modeling. However, measuring accurate emission at high temperatures remains a challenge. A new micro-furnace design was created to integrate with a Fourier transform infrared spectrometer, replacing the previous furnace and improving the performance and error metrics. Importantly, this approach accounts for all significant error sources and uses only one spectrometer to acquire sample and calibration emission data over greater temperature (473–1,573 K) and spectral (4,000–500 cm^{-1}, 2.5–20 μm) ranges. Emissivity spectra of forsterite and quartz samples were acquired to test the calibration procedure. Forsterite, with no expected phase transitions over the temperature range, showed spectral change above ~1140 K, potentially due to amorphization–a process not well described in past studies. The quartz results revealed the expected polymorph transformations at ~846 and ~1323 K. A Hawaiian basalt sample served as a representative rock test and showed an increase in emissivity (~25%) with decreasing temperature. The greatest emissivity increase (~60%) occurred in the middle infrared region (3,333–2,000 cm^{-1}, 3–5 μm). This is significant for thermal/mass flux calculations using satellite data in this spectral region, which rely on emissivity to derive accurate temperatures. All results are consistent with our previous investigations, but with improved mean accuracy (<2%), uncertainty (<4%), and spectral contrast (<20%). The improved metrics were achieved by constraining the sample measurement geometry, sample temperature stability, and environmental contamination within the experiment.

Plain Language Summary Acquiring high temperature laboratory-based infrared emission spectra of geologic samples is important to constrain their thermal and spectral properties. However, these measurements are challenging to acquire accurately. These measurements are increasingly important in calculations of lava flow cooling, crust formation rates, and ultimately lava flow propagation modeling. A new micro-furnace was created to integrate with an existing Fourier transform infrared spectrometer, replacing the previous furnace and improving the performance metrics. Importantly, unlike other recent laboratory studies, this approach accounts for all significant error sources and uses only one spectrometer to acquire both sample and calibration emission data over greater temperature and spectral ranges. Critically, the calibration can be directly tied to well-established emissivity measurements at lower temperatures validating the approach. Emissivity spectra of forsterite and quartz samples were acquired to test the calibration procedure and validated the approach. The mineral results revealed the expected polymorph transformations and potential amorphization of the crystal lattice–a process not well described in past studies. A Hawaiian basalt sample served as a representative rock test and showed an increase in emissivity with decreasing temperature. This is significant for satellite data acquired in this spectral region, as they rely on emissivity to derive accurate temperatures.

1. Introduction

Emission spectroscopy provides a quantitative analytical technique for studying geological materials through laboratory, field, and remote sensing approaches (e.g., King, McMillian, et al., 2004; King, Ramsey, et al., 2004; Swayze et al., 2004). Emissivity is an intrinsic property of a material and was defined as the ratio

of the radiant energy emitted by that surface compared to that emitted by a blackbody (a perfect emitter) at the same temperature. Emission spectroscopy measures the vibrational modes that occur within the molecular structures of materials (e.g., McMillan, 1985) and therefore is primarily used in the geosciences to identify minerals (e.g., Christensen et al., 2000; Ruff et al., 1997). For example, aluminosilicate, carbonate, sulfate, and oxide bonds are the primary cause of diagnostic absorption features (emissivity lows) observed in the middle and thermal infrared (MIR and TIR) spectra (3,333-500 cm^{-1}; e.g., King, Ramsey, et al., 2004; McMillan, 1985; Vaughan, 1989). The emissivity spectra of natural surfaces, analyzed with techniques such as linear spectral deconvolution, reveal the specific mineral composition, micron-scale roughness, particle sizes, and morphological textures (e.g., Carter et al., 2009; Ramsey & Christensen, 1998; Ramsey & Fink, 1999; Rose et al., 2014).

Emission spectroscopy can also be used to understand and quantify how efficiently radiant energy is emitted (Harris, 2013; Thompson & Ramsey, 2020). Characterizing changes in emissivity that occur with temperature and physical state (solid and liquid) is important for accurately calculating the thermal heat budget of a surface (e.g., heat flux) and any subsequent modeling based on it (Harris, 2013; Thompson & Ramsey, 2021). In volcanology, emission spectroscopy has improved numerous studies by resolving more accurate temperatures, which over time, reveals precursory activity and other derived properties (e.g., composition and heat flux; Harris, 2013; Ramsey & Harris, 2013). For example, in lava flow propagation modeling, improved estimates of radiant emission efficiency using more accurate emissivity data, can improve calculations of cooling rates and crust formation (Ramsey et al., 2019; Thompson & Ramsey, 2021). Furthermore, there is an equally important application in the spectral analysis of minerals or rocks. The spectroscopic changes seen with increasing temperature and phase transitions is directly related to the molecular structural changes, and how these changes affect emission measurements should be quantified. Therefore, improving the methodology for acquiring quantitative, well-calibrated emission spectra in the laboratory of geological samples over a wide range of temperatures is important for MIR and TIR remote sensing and the volcano science that relies on these data.

In this investigation, we developed an entirely new micro-furnace to integrate with an existing Fourier transform infrared (FTIR) spectrometer to acquire quantitative, reproducible, and accurate emissivity spectra of minerals and rock samples from 473 to 1,573 K. This temperature range was targeted to evaluate all emissivity changes through the solidus, glass transition, and liquidus temperatures for the majority of extrusive volcanic lavas observed on Earth and other planetary bodies. The furnace design is based on the previous work by Lee et al. (2013), but is smaller and most importantly, improves the integration with long-accepted emissivity calibration processing methodology (e.g., Glotch & Rogers, 2013; Ruff et al., 1997; Williams & Ramsey, 2019). These improvements better constrain the sample optical geometry (by using a triple-axis positioning system), sample temperature stability (with improved insulation), and environmental contributions (downwelling radiance knowledge and removal). Similar to the Ruff et al. (1997) study, we performed a thorough calibration with error and uncertainty analysis to evaluate the accuracy of the results. The new micro-furnace was first tested and validated using two mineral samples, whose spectra were well documented in the literature. A basalt rock sample was then analyzed, and the results document the change in emissivity during cooling from a molten to a glassy surface. Ultimately, evaluating the dependency of emissivity on temperature across a variety of geological materials, including active lava, will result in more accurate temperature data as well as improved compositional retrievals of these high temperature surfaces.

2. Background

Typically, there are three major limitations for accurately determining the emissivity of high temperature surfaces using remote sensing; the spatial, spectral, and temporal resolution of the data (Ramsey & Harris, 2013). For example, there are numerous Earth orbiting TIR instruments (e.g., Advanced Spaceborne Thermal Emission and Reflection Radiometer [ASTER] and ECOsystem Spaceborne Thermal Radiometer Experiment on Space Station [ECOSTRESS]) that acquire multispectral emissivity data, but the spatial and temporal resolutions are moderate (>60 m and >1 day), making it almost impossible to detect spatiotemporal changes in surface emissivity of active lava flows. Also, until recently, common ground-based TIR cameras have lacked any multispectral capability, precluding the ability to measure the emissivity (e.g., Ito et al., 2018; Thompson & Ramsey, 2020; Thompson et al., 2019). Therefore, there has been a major focus to

improve the analytical capacity of making accurate high temperature emission measurements in the laboratory for applications to remote sensing data (Biren et al., 2020; Lee et al., 2013; Lombardo et al., 2020).

The ability to acquire hyperspectral emissivity data over a wide range of temperatures requires a well-calibrated laboratory procedure, which limits any measurement bias and ultimately improves remote sensing analysis (Harris, 2013; Ruff et al., 1997). Most laboratory studies do not acquire data simultaneously in the MIR and TIR regions due to instrument limitation or the focus of the study. However, because of the large range of surface temperatures present on active volcanic surfaces, there is a correspondingly large change in thermal emission over this spectral range. One solution is to develop a furnace experiment that integrates with a FTIR spectrometer to acquire emissivity spectra over the range of surface temperatures and physical states present in volcanic systems. This experiment was first developed by our group to investigate emissivity changes of high silica glasses during melting and cooling across the glass transition (Lee et al., 2013). These results, using the early prototype of the micro-furnace integration with a FTIR, did capture the changes in emissivity absorption band wavelength position, however, the band depth changes with temperature were only relative.

Laboratory measurements of emissivity, as opposed to acquiring reflectance and converting that into emissivity using an assumption (e.g., Kirchhoff, 1860), are not trivial and the ability to make those measurements accurately over a large range of temperatures requires an understanding of all possible error sources. For example, downwelling radiance is the energy from the environment and instrument that reflects off the sample that is, measured by the detector. These energy sources, typically non-blackbody and non-isothermal, result in a decrease in the spectral contrast if not accurately identified and removed. Previous work at temperatures <350 K used a temperature stabilized sample chamber to reduce these energy sources and produce highly accurate results (e.g., Ruff et al., 1997). Other more recent studies have developed methodologies to acquire emissivity of materials at high temperatures for a range of applications from volcanology to planetary science (Biren et al., 2020; Lombardo et al., 2020; Maturilli et al., 2019). These studies have been successful at measuring surfaces over a limited spectral and temperature range, however without addressing all sources of error, most notably downwelling radiance. For example, high temperature emissivity spectra of mafic samples across glass transition temperatures were made in the laboratory by Lombardo et al. (2020). Their methodology does not provide a robust and easily repeatable approach to account for environmental and instrumental radiance contributions accurately. This leads to spectra with lower spectral contrast similar to our earlier studies (Lee et al., 2013). Other studies by Biren et al. (2020) and Maturilli et al. (2019) either use multiple spectrometers, external blackbodies, and/or calibration approaches that do not capture the full range of error sources. For example, Maturilli et al. (2019) use induction to heat samples to 900 K and derive emissivity by dividing the sample measurement by that of the blackbody consisting of blast furnace slag material. This qualitative approach will miss error terms caused by downwelling radiance and could introduce spectral artifacts from non-blackbody behavior. The induction heating approach also limits the high temperature range to sub-liquidus temperatures for most geological samples, as their work focused on planetary relevant studies.

3. Methodology

3.1. Experiment Setup

The new micro-furnace was developed to heat mineral and rock samples to temperatures between 473 and 1,573 K. It was designed to integrate with an existing Nicolet Nexus 670 FTIR spectrometer set-up allowing quantitative emission spectra of samples over the 4,000–500 cm^{-1} (2.5–20 μm) spectral range during heating and/or cooling. The micro-furnace was incorporated into the existing external atmospherically controlled experiment chamber of the FTIR spectrometer and relies upon the same off-axis parabolic mirror as the low temperature configuration. The mirror redirects the emitted energy from the sample through an open port into the spectrometer to a liquid nitrogen cooled mercury cadmium telluride (MCT-B) detector with a XT-KBr beam splitter. The spectrometer and external experiment chamber (including the micro-furnace) are housed within a dry air (H_2O and CO_2–scrubbed to less than 1% relative humidity) environment to limit any atmospheric contamination during data acquisition. The spectrometer has a minor positive pressure to prevent any contamination from the external experiment chamber.

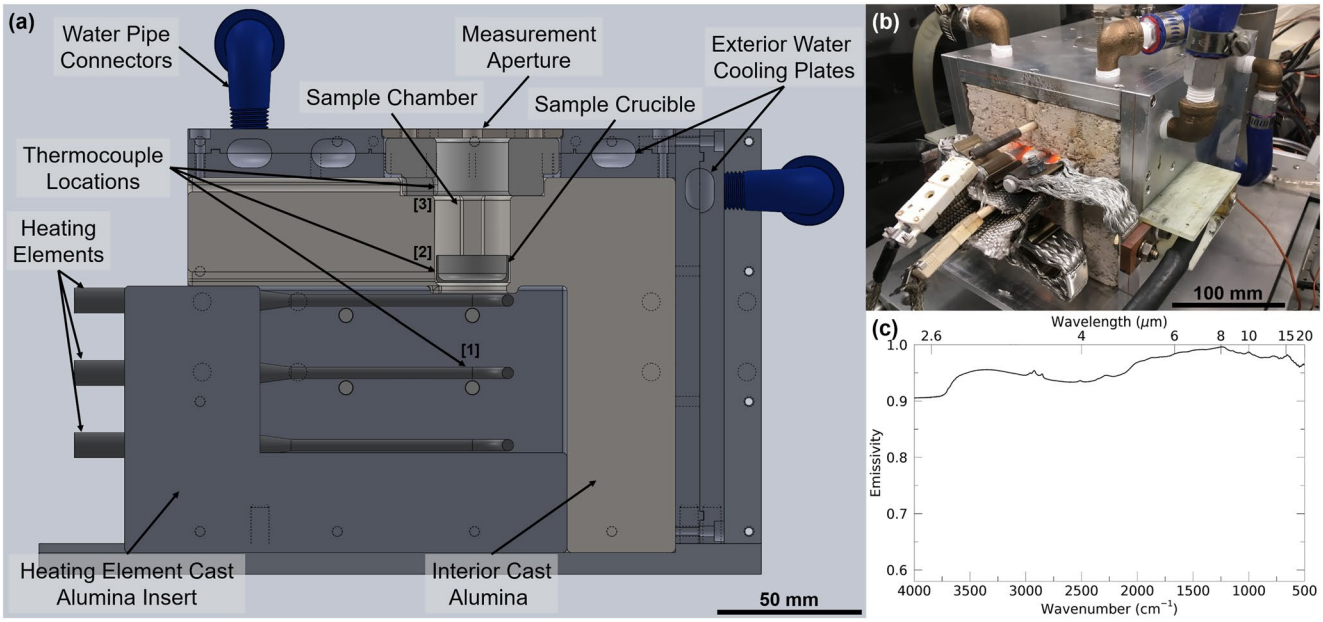

Figure 1. (a) The cross section CAD assembly model of the new micro-furnace developed to integrate with the existing Nicolet Nexus 670 Fourier transform infrared (FTIR) spectrometer. Emitted energy from the hot sample passes up through the small hole in the removable aperture to the off-axis parabolic mirror, where it is redirected into an external open port of the spectrometer to the detector. The numbers in square brackets indicate the position of the thermocouples referenced in the text. (b) The completed micro-furnace assembly, operating at a sample temperature of 1,373 K. (c) Emissivity spectrum of the cast alumina (Al_2O_3) used for the insulation and as the calibration reference standard. Data were acquired using reflectance measurements of the alumina (Hamilton, 2018) and confirmed with our standard FTIR setup at ~353 K (Williams & Ramsey, 2019). The emissivity spectrum varies by <2% in the thermal infrared (TIR) region and <9% over the entire spectral range, with errors of <2% (Hamilton, 2018).

Sample temperatures in the micro-furnace assembly are accurately achieved using three molybdenum disilicide ($MoSi_2$) heating elements controlled by two Type-B thermocouples (+/− 0.5%; Figure 1a: [1] and [2]). The heating elements are housed directly beneath the furnace sample chamber within cast alumina (Al_2O_3) ceramic insulation and so are not used to directly measure the sample temperatures. The thermocouples were positioned within the heating element chamber and at the sample crucible surface to maintain accurate furnace and sample temperatures during data acquisition (Figure 1). A water cooling system encases the insulation to reduce overheating and maintain a consistent outside environment temperature. The entire micro-furnace is positioned atop a triple-axis leveling system to guarantee that the sample surface is precisely located at the focal point of the external off-axis parabolic mirror.

The sample chamber was housed within the alumina insulation directly above the heating element hot zone. A removable small diameter (9 mm) aperture is placed above the sample chamber to limit the amount of sample radiance reaching the detector as well as reduce any downwelling environmental radiance (Figure 1). The chamber and aperture together prevent emission from external energy sources (e.g., walls, ceiling, and lights) that could contribute to the sample measurement. With this configuration, the downwelling energy comes only from the chamber walls, which have well known and well controlled properties (temperature and emissivity). This creates a similar design concept to the temperature-controlled sample chamber used for our lower temperature thermal emission spectroscopy measurements and described by Ruff et al. (1997). A third thermocouple is positioned within the sample chamber (Figure 1a: [3]) to measure the temperature contribution of the chamber walls (alumina). This chamber design, minus the sample, also serves as the blackbody calibration source, allowing all required measurements to be made with the same spectrometer and a common configuration. With the addition of the aperture, the larger chamber (~35 mm dimeter, ~40 mm depth) below behaves like a classic pinhole blackbody cavity that absorbs the majority of reflected energy after the first internal reflection.

3.2. Acquisition Technique

The technique developed to acquire calibrated micro-furnace emissivity spectra of samples was adapted, using the same nomenclature, from the methodology described by Ruff et al. (1997). Emissivity of the sample ($\varepsilon_{\text{samp}}$) is calculated using Equation 1, as a function of wavelength (λ) and temperature (T) for all parameters:

$$\varepsilon_{\text{samp}}\left(\lambda,T\right)=\frac{\frac{V_{\text{meas}}\left(\lambda,T\right)}{F}-\varepsilon_{\text{env}}\cdot B_{\text{env}}\left(\lambda,T\right)+B_{\text{inst}}\left(\lambda,T\right)}{B_{\text{samp}}\left(\lambda,T\right)-\varepsilon_{\text{env}}\cdot B_{\text{env}}\left(\lambda,T\right)} \tag{1}$$

where V_{meas} is the voltage measured by the MCT-B detector, $\varepsilon_{\text{env}}B_{\text{env}}$ is the downwelling radiance contribution from the alumina (using the temperature recorded by the sample chamber thermocouple and the known emissivity of the cast alumina insulation Figure 1). The spectrum of the cast alumina was made using a Thermo Scientific iN10 Fourier transform infrared microscope (μ-FTIR) that measures bi-directional reflectance spectra from 4,000 to 400 cm^{-1} (2.5–25 μm) following Hamilton (2018) and converted to emissivity using Kirchhoff's law. The emissivity of the cast alumina is incorporated directly into the environment calculations, which differs from Ruff et al. (1997), who assume perfect blackbody emission at the measured chamber temperature (~298 K). The emissivity variability of the alumina is low over the entire wavelength region (<9%) and thermally stable making the downwelling correction straightforward. The contribution of the environment on the sample measurement is especially important for high temperatures as this contribution can be a considerable fraction of the total emission measured. B_{inst} represents the radiance contribution from the instrument that does not originate from the sample, and B_{samp} is the radiance of the sample. F is the response function of the spectrometer, which is calculated by measuring a blackbody at two different known temperatures using the following Equation 2:

$$F=\frac{V_{bb}\left(T_1\right)-V_{bb}\left(T_2\right)}{\varepsilon_{bb}B_{bb}\left(T_1\right)-\varepsilon_{bb}B_{bb}\left(T_2\right)} \tag{2}$$

where V_{bb} is the measured detector voltage of the blackbody at two temperatures. B_{bb} is the radiance of the blackbodies at those same temperatures, calculated using the Planck equation with the known emissivity and measured temperatures. Typically, the temperatures of the blackbody measurements bracket the desired sample temperature. The instrument radiance contribution (B_{inst}) is then calculated using one of the blackbody measurements and the response function in Equation 3.

$$B_{\text{inst}}=\varepsilon_{bb}B_{bb}-\frac{V_{bb}}{F} \tag{3}$$

$$B_{\text{samp}}\left(CF\right)=\frac{V_{\text{samp}}\left(CF\right)}{F}+\varepsilon_{\text{inst}}B_{\text{inst}}\left(CF\right) \tag{4}$$

The radiance of the sample (B_{samp}) is calculated in Equation 4 by assuming a sample emissivity of 1.0 near the Christiansen Frequency (CF), where the index of refraction of the sample is equal to that of the surrounding medium (Henry, 1948). Therefore, no downwelling radiance contributions affect the measurement and so are ignored, as emissivity is assumed to be one (Figure 1c). By definition, the maximum sample temperature is derived at the CF using the Planck equation. Finally, these variables are arranged in Equation 1 to determine the emissivity spectrum of the sample accounting for the contributions of all error terms.

3.3. Data Acquisition Procedure

The methodology for acquiring the high temperature emissivity spectra of samples begins by collecting a set of blackbody measurements at ±50 K increments above and below the expected sample set temperatures (e.g., 550 and 650 K for an expected sample temperature measurement at 600 K). Unlike lower temperature emissivity measurements that use external calibrated blackbodies (Lee et al., 2010; Ruff et al., 1997) or other high temperature experiments that use commercial blackbodies measured by a second spectrometer

(Biren et al., 2020; Lombardo et al., 2020; Maturilli et al., 2019), we utilize the sample chamber itself as the blackbody source taking advantage of the pinhole configuration (e.g., Donaldson Hanna et al., 2017, 2021; Thomas et al., 2012). These measurements are used to determine the instrument response function (F) and instrument radiance contributions (B_{inst}) in Equations 3 and 4. A cast alumina ceramic disk, the same material used for the micro-furnace insulation, is then used instead of a sample and placed in the platinum (Pt) sample crucible within the micro-furnace sample chamber. This material has the same well-defined emissivity spectrum shown in Figure 1c (Hamilton, 2018). This spectrum combination with sample chamber design and small measurement aperture produces blackbody radiance that does not change up to 2345 K.

After all the desired blackbody measurements are collected, the system is allowed to cool, and the alumina disk is replaced by a 2–3 mm thick layer of sample in the crucible. The samples are typically crushed by hand and sorted to particle sizes of 100–350 μm. This depth and particle size were chosen to limit sample anisothermality (1–5 K) and melt creep/crucible overflow during the experiment. However, other thicknesses and particles sizes are possible but longer equilibration times and sample care are required. Platinum is chosen for the sample crucibles because of its common use in other high temperature experiments. It does not oxidize or react with the samples at the collection temperatures used in this experiment. Sample measurements are typically acquired at 100 K intervals and can be collected during heating or cooling (or both) of the sample. The rate of heating and cooling can also be varied dependent on the study, with a rate of ∼400 K/hr used in this study. An equilibration time of 4–5 min is used at each acquisition temperature to ensure the sample is at thermal equilibrium (sample temperatures vary by <±10 K) before the start of data acquisition. During these heating and equilibrium periods, the aperture hole is covered to improve the heating efficiency and reduce excess heat loss into the environment. This cover is then removed and spectral acquisition occurs for 10 s (8 scans), with no detectable cooling of the furnace occurring. Eight scans were chosen because the intense sample radiance provides high signal to noise (comparable to 256 or 512 scans for our 353 K standard measurements) as well as to prevent the detector and environment heating at the higher temperatures.

Despite the limited exposure time of each hot sample measurement, the temperature of the spectrometer itself can change over time. This causes calibration errors especially where using uncooled detector systems (Ruff et al., 1997). This is less of a concern for our configuration with the cooled detector. However, to reduce these errors and increase the accuracy of results, blackbody measurements are acquired again after the series of sample collections. This provides information about any instrument temperature drift over time and ensures they are correctly removed. Additionally, the temperature of the sample chamber is recorded during each spectral acquisition to account for any change to the contribution of downwelling radiance from the chamber itself on the sample measurements.

3.4. Samples

The accuracy of the new micro-furnace measurements was validated first using two laboratory mineral sample standards: forsterite (Mg_2SiO_4) and quartz (SiO_2). The quartz sample was acquired from Ward's Science as ∼10 cm long crystals that were analyzed to be 99.9% pure. The forsterite sample was collected from the Newdale olivine deposit located east of Micaville, Yancey County, North Carolina. The bulk mineral chemical composition is 41.06 wt.% SiO_2 with a Fo# of 96.3 (Hunter, 1941). The quartz and forsterite samples were crushed and sieved to 100–350 μm particle size fraction; washed with acetone (to remove clinging fines); and dried in an oven at ∼350 K for at least 24 h. These samples were chosen because of their long history in spectral investigations and representation in spectral libraries (Baldridge et al., 2009; Christensen et al., 2000), as well as their well-documented phase transitions (e.g., quartz) or lack thereof (e.g., forsterite) across the range of experiment temperatures (Hamilton, 2010; Heaney et al., 1994; White & Minser, 1984). Additionally, the spectral results achieved at the lower furnace temperatures could be compared with the spectra of the same samples acquired using our standard acquisition configuration (e.g., Williams & Ramsey, 2019) at a lower temperatures (353 and 458 K) and the same experimental methodology developed by Ruff et al. (1997).

Finally, measurements were acquired of a Hawaiian basalt sample from Kīlauea volcano. The sample was collected from the Pu'u Ō'ō episode 61 g lava flow on January 30, 2018 (19.34971°N, 155.04752°W). The bulk

rock chemical composition is 50.8 wt.% SiO_2 with a Mg# of 0.38 (Chevrel et al., 2018). The sample was also crushed and prepared in the same way as the mineral samples.

3.5. Error and Uncertainty Analysis

A detailed analysis of the random and systematic errors associated with the spectral measurements using the micro-furnace experiment was also conducted to determine the difference between a measurement and the true value of the measurement. Uncertainty was characterized to quantify the range of values within which the true value is asserted to lie with some level of confidence. The methodology for determining errors and uncertainty follow the exact techniques described by Ruff et al. (1997). Errors were quantified by varying the input parameters in the calibration to assess any deviation from reference synthetic emissivity spectra. The quartz sample was used in the uncertainty analysis as done in the previous study by Ruff et al. (1997).

The error analysis varied the calibration input parameters separately to determine any change in the derived emissivity spectrum that arose due to errors in each of the input parameters. Two synthetic reference spectra were used to discern any difference between the known reference emissivity and the results derived by varying the input parameters. Two constant synthetic emissivity spectra were generated as the references: a blackbody ($\varepsilon = 1.0$) and a graybody ($\varepsilon = 0.5$). These can establish any wavelength-dependent errors at a constant emissivity and also evaluate any emissivity dependent errors. The synthetic spectra were generated by using Equation 1 rearranged to solve for $V_{\text{meas}}(\lambda,T)$, using a variety of set temperatures (473–1573 K) and the constant emissivities of 1.0 and 0.5. Then, the raw spectra ($V_{\text{meas}}(\lambda,T)$) were calibrated using Equation 1 to produce the synthetic emissivity spectra. The errors associated with the calibration procedure were assessed by changing the input parameters individually to the maximum error values expected during the experiment and data acquisition. The maximum errors were assessed from the instrument's sensitivity derived from manufacturer specifications and reasonable expectations for the experiment (comparable to expectations in Ruff et al. (1997)). For example, the manufacturers supplied accuracy errors of the thermocouples used to obtain temperatures in the micro-furnace. These values were used in the calibration of the raw synthetic spectra ($V_{\text{meas}}(\lambda,T)$) and any deviation of the processed error spectra from the reference spectra was normalized and quantified using the following Equation 5:

$$\Delta\varepsilon(\%) = \frac{(\varepsilon_{\text{err}} - \varepsilon_{\text{ref}})}{\varepsilon_{\text{ref}}} \cdot 100 \tag{5}$$

where $\Delta\varepsilon$ is the difference between the error and reference emissivity spectra, ε_{err} is the error emissivity spectrum, and ε_{ref} is the known reference spectrum (either blackbody or graybody). These errors were combined and propagated through the calibration procedure to determine the total errors associated with this experiment.

Next, the uncertainty analysis was achieved by calculating the standard deviation between multiple quartz spectra acquired across the temperature range of the experiment. The variation was calculated from 12 repeat measurements at each measurement temperature over a 3-month time period. The standard deviation was determined over the 12 repeat spectra at each temperature and then averaged. This characterizes the range of values within which the true value lies.

4. Results and Discussion

4.1. Mineral Samples

The forsterite spectra acquired at the lowest temperatures (350–450 K) possible with the micro-furnace show nearly identical spectral features as those acquired using our standard acquisition procedure (Williams & Ramsey, 2019), thus confirming the micro-furnace configuration and calibration (Figures 2a and 2b). For example, the difference between the hottest standard experiment forsterite spectrum (458 K) and coolest furnace experiment forsterite spectrum (473 K) is 1.13% over the entire spectral range. The strong forsterite reststrahlen band absorption (emissivity minima from ~0.8 to ~0.93) is observed at ~940 cm^{-1} (~10.64 μm), with another strong absorption band (emissivity minima from ~0.91 to ~0.96) at 1,050 cm^{-1} (9.52 μm;

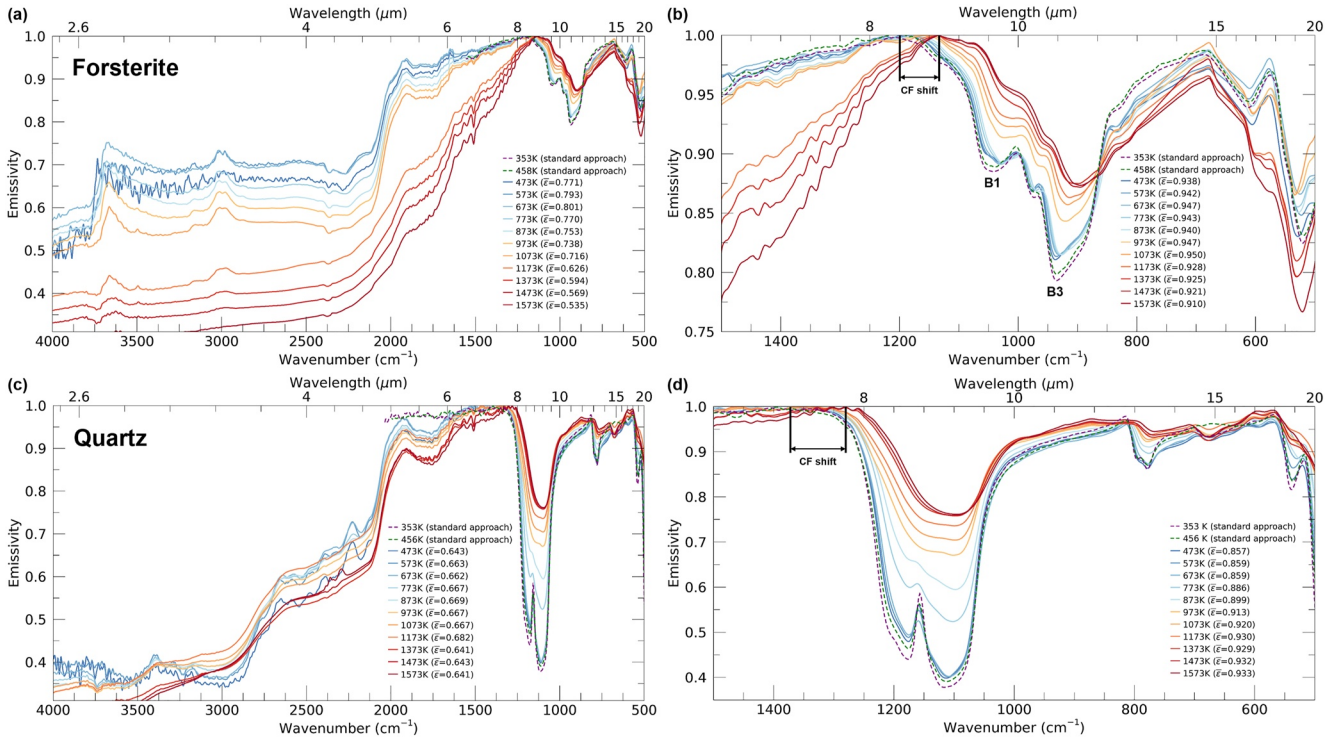

Figure 2. Emissivity results of the mineral samples with 100–350 μm particle size during heating from 473 to 1573 K. (a and b) The forsterite data show the strong reststrahlen band absorption feature centered at ~950 cm^{-1} (~10.53 μm) with a similar overall shape to the spectrum acquired at 353 and 458 K using our standard approach configuration (purple/green dashed line). The band numbers are from reflectance data by Hamilton (2010). (c and d) The quartz data show the strong reststrahlen band doublet between ~1240 cm^{-1} and 1,050 cm^{-1} (~8.06 and 9.52 μm) and a similar shape to the spectrum acquired at lower temperatures (purple/green dashed line). (b and d) thermal infrared (TIR) region shown at a different scale to highlight the features in this region, which is important for aluminosilicate identification and thermal regime analyses. $\bar{\varepsilon}$ represents the mean emissivity value for the corresponding temperature across the entire wavelength range of each plot. Total errors are less than 4% for all temperatures and wavelengths. The noise at lower temperatures in the middle infrared (MIR) region is due to only eight scans per acquisition.

Figure 2b). There are also weak absorption features in the reststrahlen band and intraband regions at 1,600 cm^{-1} (6.25 μm), 975 cm^{-1} (10.25 μm), and 620 cm^{-1} (16.13 μm). These features are consistent with previous spectral measurements (Baldridge et al., 2009; Christensen et al., 2000; Hamilton, 2010) and can be observed at all temperatures (Figure 2b), but the absorption decreases (~5–10%) at higher temperatures. In the TIR region, there is a ~1% absorption change in spectra between 473 and 873 K and 1,173–1573 K, with a ~3% absorption change observed between 873 and 1173 K measurements (Figure 2). There should not be any major spectral changes in forsterite across this temperature range because of the lack of a phase transition (Eckes et al., 2013). The changes observed here are attributed to both iron (Fe) oxidation of the sample as well as possible amorphization of the forsterite atomic lattice during rapid heating. The minor amount of Fe (as geochemically the sample is not 100% forsterite) can cause the spectral contrast to decrease in the TIR (<11%) at around 1140 K (Michel et al., 2013). The loss of spectral features at higher temperatures is more akin to amorphization in glasses despite the sample being well below the liquidus temperature. Only a few prior studies have observed amorphization of olivine caused by different processes including thermal annealing (Brucato et al., 2004; Devanathan et al., 2007). We are likely seeing a similar result here, but further FTIR studies of these spectral changes are needed to provide clarity into this process. Additionally, a shift of 51 cm^{-1} (4.3%) in the CF position is observed over the temperature range. Overall, the spectra acquired have emissivity and spectral shapes similar to those expected (Figures 2a and 2b).

The quartz sample was also used to validate the new experiment and showed similar results to those seen for the forsterite, with comparable results to our standard acquisition temperature (353 and 456 K) spectra (Figures 2c and 2d). For example, in the TIR region, the lower temperature furnace results (<673 K) are similar to the highest temperatures (353 and 456 K) achievable with our standard measurement approach, but have slightly lower spectral contrast (1.56%) as a result of the difference in uncertainties between the

two experiments (Figures 2c and 2d). At lower temperatures (<800 K), the spectral features observed are consistent with previous spectral measurements (Baldridge et al., 2009; Christensen et al., 2000). Quartz is more temperature sensitive than forsterite as different polymorphs form at higher temperatures. During our experiment, we would expect the pure α-quartz to transform to β-quartz at ~846 K and β-quartz to transform to β-cristobalite at ~1323 K during heating (Heaney et al., 1994). The reststrahlen band absorption doublet is observed between ~1240 cm^{-1} (~8.06 μm) and 1,050 cm^{-1} (9.52 μm) with emissivity minima varying from ~0.4 to ~0.8. There are also weak absorption features (emissivity minima between ~0.88–0.97) at 3,750 cm^{-1} (2.66 μm), 1,800 cm^{-1} (5.55 μm), 780 cm^{-1} (12.82 μm), and 540 cm^{-1} (18.52 μm; Figure 2). Generally, the spectral contrast of the absorption features decreases (~11%) with increasing temperature (from 473 to 1573 K). As expected, at 873 K the sample completely transformed to β-quartz, shown by the transition of the reststrahlen band absorption from a doublet to a single feature between ~1240 cm^{-1} and 1,050 cm^{-1} (~8.06 and 9.52 μm). This result is consistent with those from other studies (e.g., De Sousa Meneses et al., 2014; Maturilli et al., 2019), however our results have a greater spectral contrast in the β-quartz measurements (by ~50%), resulting from the more accurate downwelling (environment) radiance removal. In the TIR region, at temperatures greater than 1373 K the reststrahlen band absorption between ~1,240 cm^{-1} and 1,050 cm^{-1} (~8.06 and 9.52 μm) narrows and the contrast in absorption features between 600 cm^{-1} and 850 cm^{-1} (16.66 and 11.76 μm) decrease (<5%) suggesting the initial formation of β-cristobalite (Figure 2d; De Sousa Meneses et al., 2014; Heaney et al., 1994). These results differ from previous studies, however (De Sousa Meneses et al., 2014; Michalski et al., 2003). First, the purity of the quartz sample used (99.9%) lowers the transition temperature to β-cristobalite (Heaney et al., 1994), and second, these results were obtained in the stable pressure temperature conditions for β-cristobalite. Whereas, Michalski et al. (2003) acquired spectra under cristobalite metastable conditions (<543 K) and so reported the presence of the α-cristobalite polymorph. A shift in the CF wavenumber is also observed during heating, with the wavenumber decreasing by 75 cm^{-1} (5.5%). Overall, the spectra acquired have the expected emissivity, spectral shapes, and polymorph transitions at the measured temperatures.

4.2. Basalt Sample

The applicability of using the micro-furnace experiment to assess the spectral change of geological materials with temperature was also assessed. Micro-furnace emissivity spectra of a Hawaiian basalt sample from Kīlauea volcano were acquired during cooling and formation of a glassy crust (Figure 3). The basalt sample was heated to 1573 K and then cooled at a rate of 400 K/hr at 100 K intervals with a five minute hiatus to observe the change over the glass transition (1,000-900 K; Gottsmann et al., 2004) from liquid to solid (molten to glassy crust). A broad reststrahlen band absorption between ~800 and 1,100 cm^{-1} (12.50–9.09 μm) was observed in all the spectra with the spectral contrast decreasing (emissivity minima from ~0.75 to ~0.9) with cooling (the opposite behavior seen in the mineral spectra). A similar MIR absorption feature and spectral contrast trend was observed at ~1,800 cm^{-1} (5.55 μm). Generally, the spectral shape is similar to Hawaiian basalt sample results acquired at standard acquisition temperatures, from other spectral measurements up to 15 μm (Baldridge et al., 2009; Meerdink et al., 2019), and from lower spectral resolution field results (Abtahi et al., 2002; Thompson & Ramsey, 2020). At higher temperatures, the basalt spectra also have a higher spectral contrast and a more dominant reststrahlen band feature between ~800 and 1,100 cm^{-1} (12.50–9.09 μm), which indicates the silica vibrational modes associated with a basaltic melt (Figure 3). The observed silica vibrational modes are a result of lower polymerization at higher temperature, causing greater disorder within the lattice and so more energy is absorbed by the material (less emitted). This is exacerbated by more degrees of freedom in the structural movement of the material at higher (and molten) temperatures, enabling more energy to be absorbed (Lee et al., 2013). A shift in the CF wavenumber by 27 cm^{-1} (2.3%) is also observed during cooling. These features and the transition in features/contrast have been observed by previous *in situ* multispectral measurements of cooling Hawaiian basalts (Thompson & Ramsey, 2020). Overall, the emissivity of the basalt shown in Figure 3 increases by ~17% (0.644–0.775) as temperature decreased (1,573–473 K), which implies the radiative cooling of the liquid (molten) surface is less efficient (Abtahi et al., 2002; Thompson & Ramsey, 2020).

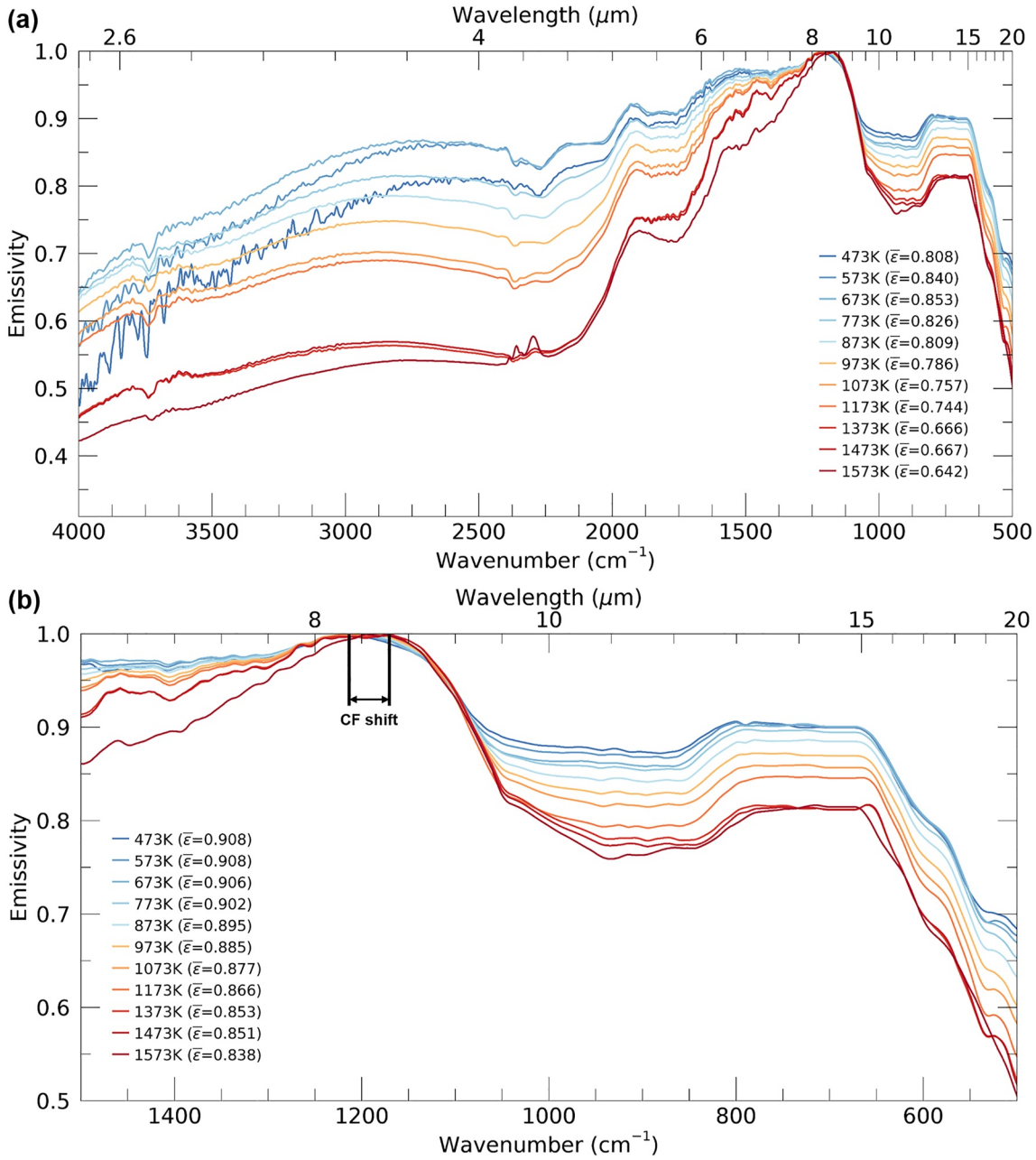

Figure 3. (a and b) Emissivity spectra acquired during cooling from 1,573 to 473 K of a Hawaiian basalt sample from Kīlauea volcano crushed to 100–350 μm. The basalt data show a broad reststrahlen band absorption feature between ~1,100 and 800 cm^{-1} (~9.09 and 12.50 μm) with the spectral contrast decreasing during cooling. (b) thermal infrared (TIR) region shown at a different scale to highlight the features in this region, which is important for aluminosilicate identification and thermal regime analyses. $\bar{\varepsilon}$ represents the mean emissivity value for the corresponding temperature across the wavelength range of each plot. Total errors are less than 4% for all temperatures and wavelengths. The noise at lower temperatures in the MIR region is a result of less signal strength and magnified by only eight scans per acquisition.

4.3. Error and Uncertainty Analysis

The measurement errors in the instrument, sample, environment, and blackbody temperatures effect on spectral emissivity accuracy were quantified using the Ruff et al. (1997) data reduction technique. These errors are explored in a rigorous way in that previous work and their methodology is followed here (Figure 4). Errors resulting from a ±5 K variation in the FTIR instrument temperature during the experiment caused <0.3% and <0.15% (4,000–500 cm^{-1}) difference in the emissivity of the synthetic spectra at the constant

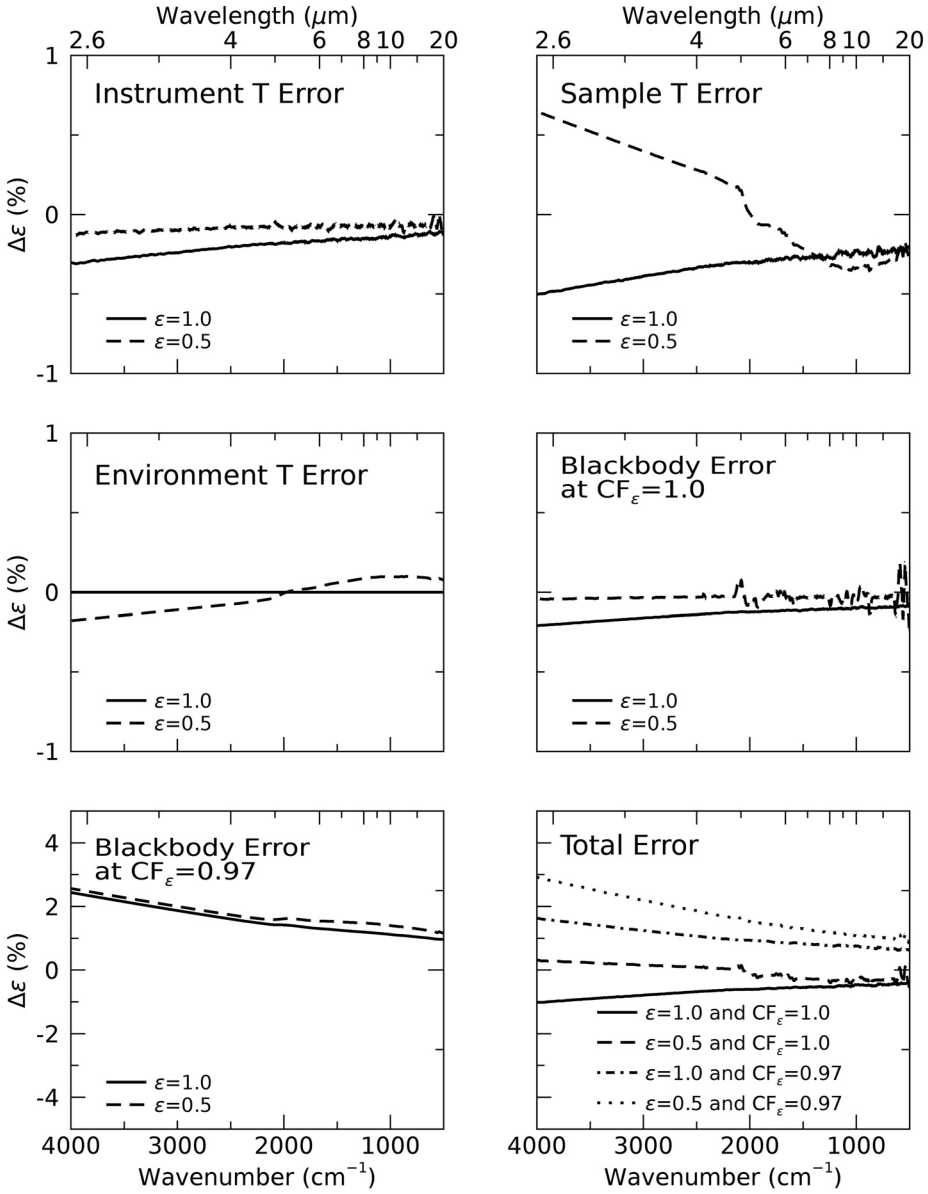

Figure 4. Contributions of error sources on the derived emissivity spectra from the micro-furnace experiment. The separate errors calculated include instrument, sample, environment, and blackbody temperature errors. The errors are means across the range of temperatures used in the experiment (473–1573 K). Therefore, the errors will vary slightly at lower and higher temperatures, respectively (see Figure 5a). The combined total errors are shown in the lower right plot.

emissivity of 1.0 and 0.5, respectively (Figure 4). Errors resulting from a ±10 K variation in the sample set temperature within the furnace caused a <0.7% (4,000–500 cm^{-1}) change in the emissivity retrieval of both the synthetic spectra (Figure 4). A ±10 K variation in the recorded environment (sample chamber within furnace) temperature resulted in no errors (4,000–500 cm^{-1}) at a constant emissivity of 1.0, and a <0.25% (4,000–500 cm^{-1}) error at a constant emissivity of 0.5 (Figure 4).

The errors associated with the blackbody calibration measurements were also assessed (Figure 4) and follows the methodology of Ruff et al. (1997). These are particularly important to the overall accuracy of the calibrated sample spectra, as these are intrinsically used to derive the instrument response function and therefore will have a large influence on the emissivity results. Errors caused by temperature inaccuracies in the blackbodies and the maximum assumed emissivity at the CF of the blackbodies were determined

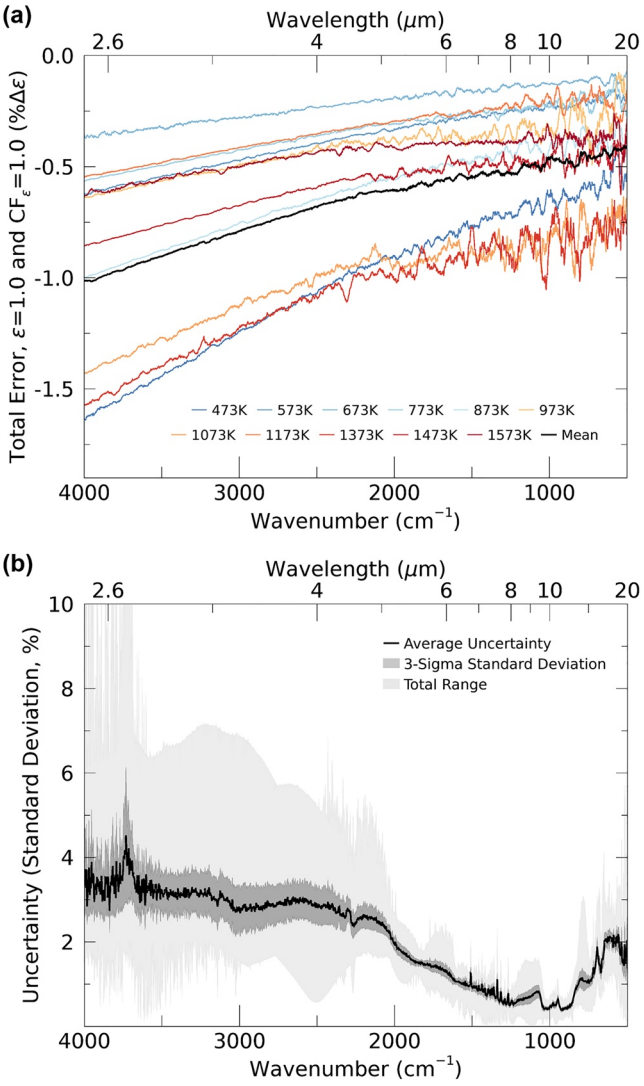

Figure 5. Plots showing the (a) total errors and (b) uncertainty (standard deviation) in the spectra acquired using the Fourier transform infrared (FTIR) spectrometer with the micro-furnace as a function of wavenumber and measurement temperature. Larger variability in errors with increasing temperatures in the TIR region reflects the typical high-frequency systematic noise of the FTIR. The mean uncertainty spectrum is an average of the entire range of temperatures used in the experiment (473–1,573 K) using 12 repeat measurement sets of the pure quartz sample.

simultaneously across the entire spectral range of the measurements (4,000–500 cm^{-1}). Errors were calculated for temperature variabilities of ±10 K from the set blackbody temperature, while simultaneously adjusting the maximum emissivity at the CF between 1.0 and 0.97. The errors resulting from a ±10 K variation in blackbody temperature with a maximum emissivity at the CF of 1.0 were <0.25% (4,000–500 cm^{-1}) in the synthetic blackbody ($\varepsilon = 1.0$) and graybody ($\varepsilon = 0.5$) spectra. A variation of ±10 K in the blackbody temperature with a maximum emissivity at CF of 0.97 caused a <2.5% (4,000–500 cm^{-1}) change in the emissivity of both the synthetic spectra (Figure 4). This is the largest source of error for this experiment. The mean total errors in the calculated emissivity using the micro-furnace were no more than a maximum of 3.0% (4,000–500 cm^{-1}), and significantly lower (<1.0%), if the exact emissivity of the blackbody is known as it is here (Figures 1c and 4). The total errors vary between ~0.1% and 1.7% ($\varepsilon = 1.0$, $CF_\varepsilon = 1.0$) with the maximum total error occurring at ~4,000 cm^{-1} (Figure 5a).

The uncertainty of the emissivity results using the FTIR spectrometer with the micro-furnace was also determined (Figure 5b). It was calculated from 12 repeat measurements at each measurement temperature over a 3-month time period. The standard deviation was determined over the 12 repeat spectra at each temperature and then averaged. This resulted in <4.0% mean variation across nearly the entire wavelength region (<2.0% in the TIR region) and the temperature range of the experiment (Figure 5b). The uncertainty varies between ~0.01% and 10% with the maximum uncertainty at ~4,000 cm^{-1} at lower temperatures and a variability between ~0.01% and 4% in the TIR region (Figure 5b).

The results from the error and uncertainty analysis are consistent with the results from Ruff et al. (1997) and are equivalent to the errors (<2%) and uncertainty (~4%; mostly <2%) calculated in their work. This is partly due to the sample temperatures being significantly higher in our experiment, resulting in the proportion of the errors being lower overall. The blackbody temperature and assumed emissivity at the CF imparted the greatest errors in the spectral measurements, as the emissivity spectrum of the cast alumina reference sample is not a perfect blackbody (i.e., $\varepsilon < 1.0$). Overall, for the majority of the results, the accuracy of the derived sample emissivity spectra (at $CF_\varepsilon = 1.0$) was <1.5% and the uncertainty was <4% (4,000–500 cm^{-1}). These are the mean values over the entire temperature range of the experiment and are worse (<70%) at temperatures lower than 673 K and improve significantly at temperatures higher than 1,173 K.

5. Conclusions

A new laboratory micro-furnace experiment was developed to integrate with an existing FTIR spectrometer to acquire accurate, high temperature emissivity spectra of geological samples. The work presented here greatly improves upon the first laboratory high temperature hyperspectral experiment developed by this group (Lee et al., 2013). The new experiment is able to acquire data over the larger 4,000 and 500 cm^{-1} (2.5–20 μm) spectral range and larger 473–1573 K temperature range. The new design improved the optical geometry of the measurement by utilizing a triple-axis precision adjustment mechanism. The furnace sample chamber is well-insulated with limited environmental interference from outside the experiment. This improved the overall stability of the sample temperature and determination of all downwelling radiance terms, resulting in more accurate error reduction and less muting of the spectra compared to our previous work (Lee et al., 2013). The data calibration follows

the long-used and well-known methodology developed by Ruff et al. (1997) and allows the blackbody targets to be referenced in the same viewing geometry and conditions as the samples. The only differences are that a cast alumina (Al_2O_3) disk is used as the blackbody reference material and the emissivity of the alumina is included in the instrument response function and environmental radiance contribution calculations. This approach coupled with the geometry of the furnace sample chamber allows the furnace itself to serve as the blackbody. This methodology provides a rigorous procedure for correcting sample measurements and deriving accurate emissivity spectra (<2% total errors) at high certainty (>96%). These were confirmed by comparing the spectra of the lowest temperatures achieved with the micro-furnace to those from the highest possible temperatures with the standard emissivity approach. These match to within 2%.

Initial testing and results from the experiment show that emissivity varies with surface temperature and physical state, as well as due to molecular structural changes (e.g., α-quartz to β-quartz polymorph transformation). The pure mineral samples (quartz and forsterite) validated the development and calibration procedure and provided new information about how emissivity varies across mineral phase transformations but with no change of state. For example, during the α-quartz to β-quartz polymorph transformation, where the crystal structure transforms from trigonal to hexagonal, a mean emissivity change of 0.013 was observed in the TIR and the strong reststrahlen band doublet absorption feature between ∼1240 cm^{-1} and 1,050 cm^{-1} (∼8.06 and 9.52 μm) changed into to a shallower single feature. The results from the forsterite showed a spectral change likely due to an amorphization process rather than any phase transition. As an expanded part of the testing and calibration procedure, a Hawaiian basalt sample from Kīlauea volcano was used to examine the effects on an igneous rock sample that did change state. The results supported previous evidence that the emissivity spectral contrast decreases and mean values increase as temperature decreases below the liquidus temperature. The results show a mean emissivity increase of ∼25% with decreasing sample surface temperatures (from 1,573 to 473 K), and a greater emissivity increase observed in the MIR (∼60%). The changes observed spectrally with temperature will have a significant influence on heat budget calculations (e.g., heat flux) that rely on radiative cooling models and hence, the emissivity of molten lava.

This work can be applied to field and remote sensing data to help identify components, glasses, and transitions of high temperature geological surfaces. Overall, the improved methodology developed for very high temperature spectral investigations of geological surfaces will have a broad impact on both the terrestrial and planetary geological communities.

Conflict of Interest

The authors declare no conflicts of interest relevant to this study.

Acknowledgments
The authors would like to thank the Machine and Electronics Shops of the Kenneth P. Dietrich School of Arts and Sciences at the University of Pittsburgh for their dedicated work fabricating the micro-furnace components. We would also like to thank Penny King for her spectroscopy expertize and insights into the calibration process and Vicky Hamilton for acquiring the reflectance measurements of the alumina. This research was funded by NASA grants 80NSSC18K1001 (Michael S. Ramsey) and 80NSSC17K0445 P00001 (James O. Thompson), and NSF Petrology and Geochemistry grant 1019558 (Michael S. Ramsey and Rachel J. Lee). We sincerely thank the two reviewers (Kerri Donaldson Hanna and Steve Ruff) and the Editor (Stephen Parman) for their helpful and constructive comments that improved this manuscript greatly.

Data Availability Statement

The calibration code is available from ASU Davinci at http://davinci.asu.edu/. The micro-furnace data are available at (Thompson et al., 2021), under a Creative Commons: Attribution-No Derivative Works 3.0.

References

Abtahi, A. A., Kahle, A. B., Abbott, E. A., Gillespie, A. R., Sabol, D., Yamada, G., & Pieri, D. C. (2002). Emissivity changes in basalt cooling after eruption from Puu Oo, Kilauea, Hawaii [abs.]. *Eos, Transactions, American Geophysical Union*, *83*(47), F1442.

Baldridge, A. M., Hook, S. J., Grove, C. I., & Rivera, G. (2009). The ASTER spectral library version 2.0. *Remote Sensing of Environment*, *113*(4), 711–715. https://doi.org/10.1016/j.rse.2008.11.007

Biren, J., del Campo, L., Cosson, L., Li, H., Slodczyk, A., & Anjujar, J. (2020). High temperature in-situ study of radiative properties of basaltic dry magmas. *European Geosciences Union*, Abs. NH6. *1*. https://www.researchgate.net/profile/Jonas_Biren/p

Brucato, J. R., Strazzulla, G., Baratta, G., & Colangeli, L. (2004). Forsterite amorphization by ion irradiation: Monitoring by infrared spectroscopy. *Astronomy and Astrophysics*, *413*(2), 395–401. https://doi.org/10.1051/0004-6361:20031574

Carter, A. J., Ramsey, M. S., Durant, A. J., Skilling, I. P., & Wolfe, A. (2009). Micron-scale roughness of volcanic surfaces from thermal infrared spectroscopy and scanning electron microscopy. *Journal of Geophysical Research*, *114*(2), 1–13. https://doi.org/10.1029/2008JB005632

Chevrel, M. O., Harris, A. J. L., James, M. R., Calabrò, L., Gurioli, L., & Pinkerton, H. (2018). The viscosity of Pāhoehoe lava: In situ syn-eruptive measurements from Kilauea, Hawaii. *Earth and Planetary Science Letters*, *493*, 161–171. https://doi.org/10.1016/j.epsl.2018.04.028

Christensen, P. R., Bandfield, J. L., Hamilton, V. E., Howard, D. A., Lane, M. D., Piatek, J. L., et al. (2000). A thermal emission spectral library of rock-forming minerals. *Journal of Geophysical Research-Planets*, *105*(E4), 9735–9739. https://doi.org/10.1029/1998JE000624

De Sousa Meneses, D., Eckes, M., Del Campo, L., & Echegut, P. (2014). Phase transformations of crystalline SiO_2 versus dynamic disorder between room temperature and liquid state. *Journal of Physics: Condensed Matter*, *26*(25), 255402. https://doi.org/10.1088/0953-8984/26/25/255402

Devanathan, R., Durham, P., Du, J., Corrales, L. R., & Bringa, E. M. (2007). Molecular dynamics simulation of amorphization in forsterite by cosmic rays. *Nuclear Instruments and Methods in Physics Research Section B: Beam Interactions with Materials and Atoms*, *255*(1 Special Issue), 172–176. https://doi.org/10.1016/j.nimb.2006.11.021

Donaldson Hanna, K. L., Bowles, N. E., Warren, T. J., Hamilton, V. E., Schrader, D. L., McCoy, T. J., et al. (2021). Spectral characterization of Bennu analogs using PASCALE: A new experimental set-up for simulating the near-surface conditions of airless bodies. *Journal of Geophysical Research: Planets*, *126*(2), e2020JE006624. https://doi.org/10.1029/2020JE006624

Donaldson Hanna, K. L., Greenhagen, B. T., Patterson, W. R., Pieters, C. M., Mustard, J. F., Bowles, N. E., et al. (2017). Effects of varying environmental conditions on emissivity spectra of bulk lunar soils: Application to Diviner thermal infrared observations of the Moon. *Icarus*, *283*, 326–342. https://doi.org/10.1016/j.icarus.2016.05.034

Eckes, M., Gibert, B., de Sousa Meneses, D., Malki, M., & Echegut, P. (2013). High-temperature infrared properties of forsterite. *Physics and Chemistry of Minerals*, *40*(4), 287–298. https://doi.org/10.1007/s00269-013-0570-z

Glotch, T. D., & Rogers, A. D. (2013). Evidence for magma-carbonate interaction beneath Syrtis Major, Mars. *Journal of Geophysical Research: Planets*, *118*(1), 126–137. https://doi.org/10.1029/2012JE004230

Gottsmann, J., Harris, A. J. L., & Dingwell, D. B. (2004). Thermal history of Hawaiian pāhoehoe lava crusts at the glass transition: Implications for flow rheology and emplacement. *Earth and Planetary Science Letters*, *228*(3–4), 343–353. https://doi.org/10.1016/j.epsl.2004.09.038

Hamilton, V. E. (2010). Thermal infrared (vibrational) spectroscopy of Mg-Fe olivines: A review and applications to determining the composition of planetary surfaces. *Chemie der Erde*, *70*(1), 7–33. https://doi.org/10.1016/j.chemer.2009.12.005

Hamilton, V. E. (2018). Spectral classification of ungrouped carbonaceous chondrites I: Data collection and processing. In: Lunar and planetary science Conference (p. 1759).

Harris, A. J. L. (2013). *Thermal remote Sensing of active volcanoes: A user's manual (first)*. New York, USA: Cambridge University Press.

Heaney, P. J., Prewitt, C. T., & Gibbs, G. V. (Eds.). (1994). *Silica: Physical behavior, Geochemistry, and materials applications*. Washington D.C.: Mineralogical Society of America. https://doi.org/10.1515/9781501509698

Henry, R. L. (1948). The transmission of powder films in the infra-red. *Journal of the Optical Society of America*, *38*, 775. https://doi.org/10.1364/josa.38.000775

Hunter, C. E. (1941). Forsterite Olivine Deposits of North Carolina and Georgia (Vol. 117). Bulletin N: Georgia Department of Natural Resources, Division of Mines, Mining and Geology.

Ito, G., Rogers, A. D., Young, K. E., Bleacher, J. E., Edwards, C. S., Hinrichs, J., et al. (2018). Incorporation of portable infrared spectral imaging into planetary geological field work: Analog studies at Kīlauea Volcano, Hawaii, and Potrillo Volcanic Field, New Mexico. *Earth and Space Science*, *5*(11), 676–696. https://doi.org/10.1029/2018EA000375

King, P. L., McMillian, P. F., & Moore, G. M. (2004a). Chapter 4 Infrared spectroscopy of silicate glasses with application to natural systems. In *Infrared Spectroscopy in Geochemistry. Exploration Geochemistry and Remote Sensing*. Mineralogical Association of Canada.

King, P. L., Ramsey, M. S., McMillan, P. F., & Swayze, G. (2004b). Laboratory fourier transform infrared spectroscopy methods for geologic samples. In: *Infrared spectroscopy in Geochemistry, exploration Geochemistry and remote sensing*. Mineralogical Association of Canada.

Kirchhoff, G. (1860). I. On the relation between the radiating and absorbing powers of different bodies for light and heat. *London, Edinburgh, Dublin Philosophical Magazine and Journal of Science*, *20*, 1–21. https://doi.org/10.1080/14786446008642901

Lee, R. J., King, P. L., & Ramsey, M. S. (2010). Spectral analysis of synthetic quartzofeldspathic glasses using laboratory thermal infrared spectroscopy. *Journal of Geophysical Research*, *115*(6), 1–9. https://doi.org/10.1029/2009JB006672

Lee, R. J., Ramsey, M. S., & King, P. L. (2013). Development of a new laboratory technique for high-temperature thermal emission spectroscopy of silicate melts. *Journal of Geophysical Research: Solid Earth*, *118*(5), 1968–1983. https://doi.org/10.1002/jgrb.50197

Lombardo, V., Pick, L., Spinetti, C., Tadeucci, J., & Zakšek, K. (2020). Temperature and emissivity separation "Draping" algorithm applied to hyperspectral infrared data. *Remote Sensing*, *12*(12), 1–16. https://doi.org/10.3390/RS12122046

Maturilli, A., Helbert, J., & Arnold, G. (2019). The newly improved set-up at the planetary spectroscopy laboratory (PSL) (Vol. 2). https://doi.org/10.1117/12.2529266

McMillan, P. (1985). Vibrational spectroscopy in the mineral sciences. In *Microscopic to Macroscopic*, (pp. 9–64). https://doi.org/10.1515/9781501508868-004

Meerdink, S. K., Hook, S. J., Roberts, D. A., & Abbott, E. A. (2019). The ECOSTRESS spectral library version 1.0. *Remote Sensing of Environment*, *230*(March), 111196. https://doi.org/10.1016/j.rse.2019.05.015

Michalski, J. R., Kraft, M. D., Diedrich, T., Sharp, T. G., & Christensen, P. R. (2003). Thermal emission spectroscopy of the silica polymorphs and considerations for remote sensing of Mars. *Geophysical Research Letters*, *30*(19), 2–5. https://doi.org/10.1029/2003GL018354

Michel, R., Ammar, M. R., Poirier, J., & Simon, P. (2013). Phase transformation characterization of olivine subjected to high temperature in air. *Ceramics International*, *39*(5), 5287–5294. https://doi.org/10.1016/j.ceramint.2012.12.031

Ramsey, M. S., Chevrel, M. O., Coppola, D., & Harris, A. J. L. (2019). The influence of emissivity on the thermo-rheological modeling of the channelized lava flows at Tolbachik volcano. *Annals of Geophysics*, *62*(2 Special Issue). https://doi.org/10.4401/ag-8077

Ramsey, M. S., & Christensen, P. R. (1998). Mineral abundance determination quantitative deconvolution of thermal emission spectra. *Journal of Geophysical Research*, *103*(10), 577–596. https://doi.org/10.1029/97JB02784

Ramsey, M. S., & Fink, J. H. (1999). Estimating silicic lava vesicularity with thermal remote sensing: A new technique for volcanic mapping and monitoring. *Bulletin of Volcanology*, *61*(1–2), 32–39. https://doi.org/10.1007/s004450050260

Ramsey, M. S., & Harris, A. J. L. (2013). Volcanology 2020: How will thermal remote sensing of volcanic surface activity evolve over the next decade? *Journal of Volcanology and Geothermal Research*, *249*, 217–233. https://doi.org/10.1016/j.jvolgeores.2012.05.011

Rose, S. R., Watson, I. M., Ramsey, M. S., & Hughes, C. G. (2014). Thermal deconvolution: Accurate retrieval of multispectral infrared emissivity from thermally-mixed volcanic surfaces. *Remote Sensing of Environment*, *140*, 690–703. https://doi.org/10.1016/j.rse.2013.10.009

Ruff, S. W., Christensen, P. R., Barbera, P. W., & Anderson, D. L. (1997). Quantitative thermal emission spectroscopy of minerals: A laboratory technique for measurement and calibration. *Journal of Geophysical Research*, *102*(B7), 14899–14913. https://doi.org/10.1029/97JB00593

Swayze, G. A., Higgins, C. T., Clinkenbeard, J. P., & Kokaly, R. F. (2004). *Preliminary report on using imaging spectroscopy to map ultramafic rocks, serpentinites, and tremolite-actinolite-bearing rocks in California*. California Geological Survey.

Thomas, I. R., Greenhagen, B. T., Bowles, N. E., Donaldson Hanna, K. L., Temple, J., & Calcutt, S. B. (2012). A new experimental set-up for making thermal emission measurements in a simulated lunar environment. *Review of Scientific Instruments*, *83*(12), 124502. https://doi.org/10.1063/1.4769084

Thompson, J. O., & Ramsey, M. S. (2020). Spatiotemporal variability of active lava surface radiative properties using ground-based multispectral thermal infrared data. *Journal of Volcanology and Geothermal Research*, *408*, 107077. https://doi.org/10.1016/j.jvolgeores.2020.107077

Thompson, J. O., & Ramsey, M. S. (2021). The influence of variable emissivity on lava flow propagation modeling. *Bulletin of Volcanology*, *83*(6), 1–19. https://doi.org/10.1007/s00445-021-01462-3

Thompson, J. O., Ramsey, M. S., & Hall, J. L. (2019). MMT-Cam: A new miniature multispectral thermal infrared camera system for capturing dynamic earth processes. *IEEE Transactions on Geoscience and Remote Sensing*, *57*(10), 7438–7446. https://doi.org/10.1109/TGRS.2019.2913344

Thompson, J. O., Williams, D. B., Lee, R. J., & Ramsey, M. S. (2021). *UPITT IVIS high-temperature FTIR data (microfurnace), dataset*. Retrieved from http://d-scholarship.pitt.edu/id/eprint/40467

Vaughan, D. J. (1989). Spectroscopic methods in mineralogy and geology. *Journal of Petrology*, *30*(6), 1541–1542. https://doi.org/10.1093/petrology/30.6.1541

White, W. B., & Minser, D. G. (1984). Raman spectra and structure of natural glasses. *Journal of Non-Crystalline Solids*, *67*(1–3), 45–59. https://doi.org/10.1016/0022-3093(84)90140-6

Williams, D. B., & Ramsey, M. S. (2019). On the applicability of laboratory thermal infrared emissivity spectra for deconvolving satellite data of opaque volcanic ash plumes. *Remote Sensing*, *11*(19), 2318. https://doi.org/10.3390/rs11192318